Rapid generation of coronaviral immunity using recombinant peptide modified nanodiamonds

Rostyslav Bilyy, Quentin Pagneux, Nathan François, Galyna Bila, Roman Grytsko, Yuri Lebedin, Alexandre Barras, Jean Dubuisson, Sandrine Belouzard, Karin Séron, et al.

pathogens

MDPI

Article

Rapid Generation of Coronaviral Immunity Using Recombinant Peptide Modified Nanodiamonds

Rostyslav Bilyy [1,*], Quentin Pagneux [2], Nathan François [3], Galyna Bila [1], Roman Grytsko [1], Yuri Lebedin [4], Alexandre Barras [2], Jean Dubuisson [3], Sandrine Belouzard [3], Karin Séron [3], Rabah Boukherroub [2] and Sabine Szunerits [2,*]

1 Danylo Halytsky Lviv National Medical University, Pekarska Str., 69, 79010 Lviv, Ukraine; halyna.bila@gmail.com (G.B.); grytskoroman@gmail.com (R.G.)
2 University of Lille, CNRS, Centrale Lille, University Polytechnique Hauts-de-France, UMR 8520-IEMN, F-59000 Lille, France; quentin.pagneux@univ-lille.fr (Q.P.); alexandre.barras@univ-lille.fr (A.B.); rabah.boukherroub@univ-lille.fr (R.B.)
3 U1019-UMR 9017-CIIL-Center for Infection and Immunity of Lille, Institut Pasteur de Lille, University of Lille, CNRS, INSERM, CHU Lille, F-59000 Lille, France; nathan.francois@ibl.cnrs.fr (N.F.); jean.dubuisson@ibl.cnrs.fr (J.D.); sandrine.belouzard@ibl.cnrs.fr (S.B.); karin.seron@ibl.cnrs.fr (K.S.)
4 Xema Co. Ltd., Akademika Efremova Str., 23, 03179 Kyiv, Ukraine; lebedin@xema.com.ua
* Correspondence: r.bilyy@gmail.com (R.B.); sabine.szunerits@univ-lille.fr (S.S.)

Abstract: Vaccination remains one of the most effective tools to prevent infectious diseases. To ensure that the best possible antigenic components are chosen to stimulate a cognitive immune response, boosting antigen presentation using adjuvants is common practice. Nanodiamond-based adjuvants are proposed here as a rapid and versatile platform for antigen conjugation, utilizing peptides common to different pathogenic strains and making this strategy a good candidate for a "ready-to-use" vaccine. Initiation of an inflammatory reaction with a resulting immune response is based on the ability of living organisms to entrap nanostructures such as nanodiamonds with neutrophil extracellular traps (NETs) formation. In this work, coronavirus peptide homological for MERS-CoV, fusion inhibitor, was conjugated to nanodiamonds and used to induce neutrophilic-driven self-limiting inflammation. The resulting adjuvant was safe and did not induce any tissue damage at the site of injection. Mice immunization resulted in IgG titers of 1/4,000 within 28 days. Immunization of rabbits resulted in the formation of a high level of antibodies persistently present for up to 120 days after the first immunization (animal lifespan ~3 years). The peptide used for immunization proved to be reactive with sera of convalescent COVID patients, demonstrating the possibility of developing pancoronaviral vaccine candidates.

Keywords: coronavirus peptide; diamond nanoparticles; neutrophil extracellular traps

Citation: Bilyy, R.; Pagneux, Q.; François, N.; Bila, G.; Grytsko, R.; Lebedin, Y.; Barras, A.; Dubuisson, J.; Belouzard, S.; Séron, K.; et al. Rapid Generation of Coronaviral Immunity Using Recombinant Peptide Modified Nanodiamonds. *Pathogens* **2021**, *10*, 861. https://doi.org/10.3390/pathogens10070861

Academic Editor: Yongjun Sui

Received: 30 May 2021
Accepted: 28 June 2021
Published: 8 July 2021

1. Introduction

Vaccines profoundly contributed to major public health breakthroughs via the management and prevention of infectious diseases [1,2]. Despite the successful use of vaccines against measles, hepatitis B, tetanus and others, there are many viral and bacterial diseases for which vaccines remain unavailable. The major challenges linked to infectious disease vaccines are linked to the choice of the nature of the epitopes against which immune response is directed [3,4].

The vast majority of vaccines available for human use are either virus or protein-based formulations. Inactivated or attenuated viruses can stimulate a robust immune response as they contain B and T-cell epitopes in a pathogen relevant conformation. Peptide and protein-based vaccines consist generally of a purified peptide/protein from the virus or virus-infected cells, or recombinant antigens. Such subunit vaccines face limitations in terms of immunogenicity and multiple injections, or the addition of adjuvants are required

to stimulate efficiently the immune system [5]. When peptide is used for vaccination, the epitope of interest is conjugated to a carrier protein or presented in a multivalent format on nanoparticles [6]. Such an approach can boost the immune system due to the immunogenic properties of the carrier.

Low-dimensional carbon-based materials (e.g., fullerene, graphene, carbon nanotubes, carbon quantum dots, nanodiamonds) recently received large attention in biomedical contexts [7–10]. Nanodiamonds (NDs) are considered in particular appealing for biomedical applications as they are less toxic than other carbon-based nanostructures [11,12]. In this context, efficient inhibition of *E. coli* adhesion to eukaryotic cells and reduction of *E. coli* biofilm formation were demonstrated using glycan-modified NDs [13–15]. NDs carrying phenylboronic acid moieties were proven to be efficient antiviral inhibitors [16]. The fluorescent properties of NDs were, in addition, used in numerous studies to tackle challenges in vaccine development [17,18]. Kossovosy et al. [19] proposed diamond nanoparticles coated with cellobiose as carrier for mussel adhesive protein (MAP) antigens for the generation of antigen-specific antibodies [19]. Pham et al. [20] used surface-oxidized diamond nanoparticles with a purified trimeric hemagglutinin (H7) protein for mice immunization and demonstrated their adjuvant properties. One important criterion in the development of nanoparticle-based adjuvants, and notably, nanodiamond-based vaccine concepts, is the effect of the size of the diamond nanoparticles on the resulting immune response [21]. Indeed, nanoparticles of diameters smaller than 40 nm were reported to get trapped in neutrophil-derived aggregates and locally orchestrate inflammation [21], and the mechanism on how nanoparticle size influence its inflammatory effect via neutrophil activation was outlined in [22]. Neutrophil mediated inflammation was also shown to be the underlying mechanism for the enhanced adjuvant properties of aluminum oxide nanowires (Al_2O_3 NWs) [23].

In this work, results of "react and inject" nanodiamond-based vaccine formulations are presented. A universal protection was reached via integration of a synthetic pan coronavirus peptide (as illustrated in Figure 1a) specific to the Middle-East respiratory syndrome coronavirus (MERS-CoV). The peptide used in this work is similar to heptad repeat 2 (HR2) peptide (HR2P-M2) reported by Lu et al. [24], an improved HR2P peptide with higher stability, solubility, and antiviral activity. The minor differences in the amino-acid sequence are identified in red, and the sequence shares 81% identify and 86% of similarity with the HR2 helix of MERS-CoV (PDB ID: 4NJL) and 46% identify and 74% of similarity with the HR2 helix of SARS-CoV-2 (as illustrated in Figure 1b); corresponding sequence alignment is represented in Figure S1. This peptide was also lately demonstrated to induce cross-coronaviral humoral immune response [25,26]. Spike protein (S protein) is mediating membrane fusion between coronaviruses such as MERS-CoV and SARS-CoV-2 and host cells [27]. While boronic-acid modified nanostructures revealed to inhibit HCoV-229E entry and the viral replication step [28], Huang et al. developed gold nanoparticles modified with a series of heptad repeat 1 (HR1) peptide inhibitors and demonstrated their ability to efficiently inhibit HR1/HR2-mediated membrane fusion between MERS-CoV and host cells [29]. We used a similar sequence of HR2 peptide inhibitor immobilized on NDs' surface via covalent bonding as well as by simple mixing. NDs conjugated with such peptide can indeed induce antibody responses when injected into the body of mice and rats and serve as a readily interchangeable component of novel vaccine.

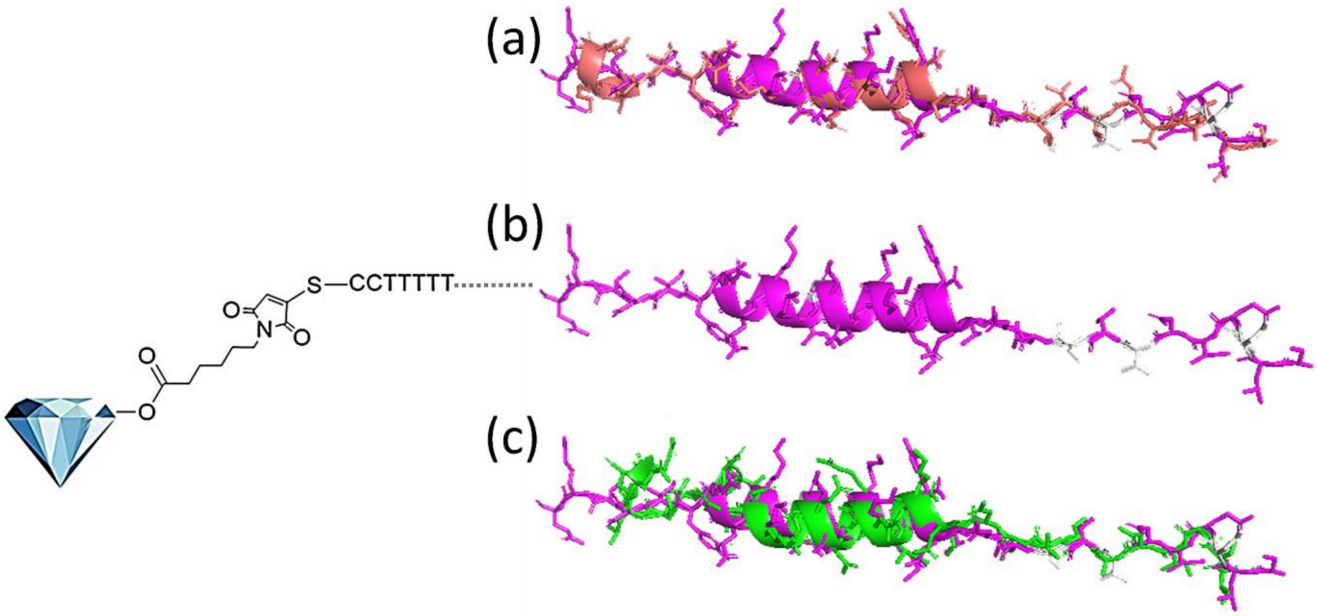

Figure 1. Pancoronavirus peptide modified nanodiamond as vaccine formulation. Diamond core with attached spacer peptide was conjugated with pancoronaviral peptide (**b**) magenta, the used peptide structure was coaligned with 3-dimensional structure of corresponding region of MERS-CoV (**a**) pink and SARS-CoV-2 (**c**) green. Used peptide possesses 86% similarity with corresponding region of MERS-CoV and 74% similarity with that of SARS-CoV-2.

2. Results and Discussion

2.1. Properties of Nanodiamond-Based Nanostructures as Vaccine Adjuvant

To validate our choice of ND as vaccine carrier, the immunogenic effect of different carbon-based materials was investigated first. Next to nanodiamonds (ND), carbon quantum dots (CQDs) derived from citric acid/ethylenediamine [28] and pegylated graphene oxide (GO-PEG) were investigated. Transmission electron microscopy (TEM) and high-resolution TEM (HRTEM) images of the employed detonation ND particles (as illustrated in Figure 2a) reveal the presence of spherical particles with a crystalline structure and an average diameter of 14 ± 5 nm (as illustrated in Figure 2b). The HRTEM image indicates a spacing of 2.3 Å corresponding to the (111) carbon lattice. The hydrodynamic diameter of these particles is 89 ± 13 nm with a zeta potential of +35.3 ± 1.6 mV (as illustrated in Table 1). The positive charge is still a point of debate, but widely observed for these diamond nanoparticles [13,30]. Indeed, XPS analysis indicates the presence of 1.5 at % nitrogen (as illustrated in Table 1) and might be responsible for the positive surface charge of ND-OH particles. The C1s core level spectrum reveals bands at 285 eV (sp^3 C-C/C-H) and bands at 285.9 eV (C-N), 286.4 (C-O) and 289.4 (O-C=O), indicating the presence of substantial amount of COOH groups on the surface of the ND (as illustrated in Figure 2c).

The transmission electron microscopy (TEM) image of the water-dispersible pegylated graphene oxide (GO-PEG) [31] shows sheet-like structures (as illustrated in Figure S2a) with an average size of 450 ± 150 nm (as illustrated in Figure S2b). The high-resolution XPS spectrum of the C1s is dominated by the band at 286.3 due to C-O/C-N bonds with two other contributions ascribed to C-Csp2 (284.5 eV), C-C/C-H (285.0 eV), and 287.8 eV (C=O) (as illustrated in Figure S2c). This contrast with the CQD used here, which exhibit a spherical shape (as illustrated in Figure S2d) of crystalline character with an average diameter of 5.1 ± 0.2 nm (as illustrated in Figure S2e) and an overall negative surface charge (as illustrated in Table 1). The HRTEM image reveals a spacing of 2.04 Å corresponding to the (111) diamond lattice. The C1s high-resolution XPS spectrum displays next to the graphitic C=C at 283.4 eV, bands at 284.9 eV (C-H) and 286.4 eV (C-O, C-N) (as illustrated in Figure S2f).

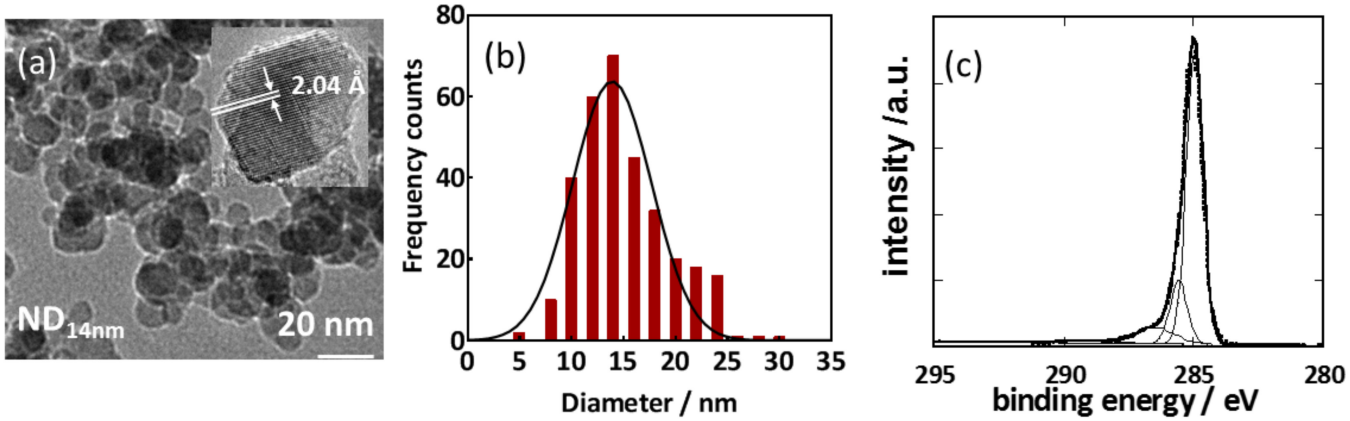

Figure 2. Characterization of nanodiamonds (NDs) used in this work: (**a**) TEM (inset HRTEM image), (**b**) size distribution, (**c**) C1s high resolution XPS spectrum.

Table 1. Physicochemical characteristics of carbon-based nanostructures.

Structure	ζ (mV) [1]	Size (nm)	Hydrodynamic Size (nm) [2]	PDI [1]	C_{1s} [3] (at. %)	O_{1s} (at. %)	N_{1s} (at. %)
ND	+35.3 ± 1.6	14.0 ± 5.0	89 ± 13	0.246 ± 0.002	88.4	10.1	1.5
GO-PEG	−25.3± 2.4	>200	-	-	75.4	22.3	2.3
CQD	−9.9 ± 3.4	5.1 ± 0.2	11 ± 0.1	0.220 ± 0.110	72.6	12.5	14.9

[1] ζ: zeta potential, PDI Polydispersity index; [2] hydrodynamic size was recorded at 37 °C; [3] XPS was used to determine atomic percentage of different elements.

None of the tested carbon particles exhibited any strong cytotoxicity on HeLa and U87MG human brain cells after 24h using the MTS assay with comparison to controls, as proposed by Kong et al. [32] (as illustrated in Figure S3). When tested for immunogenicity in a standard immunization test employing ovalbumin as antigen, only NDs exhibited strong immunomodulatory action using the experimental design, as presented in Figure 3a. Nine groups of Balb/C mice, each of 5 to 8 animals, were immunized by intraperitoneal injection (i.p.) at day 1 and 14 with one of the nanostructures (CQD, GO-PEG or ND) mixed with 50 μg chicken ovalbumin (OVA) as model antigen. Analysis of humoral immune response (as illustrated in Figure 3b) demonstrated that immunization with any of these particles triggered production of anti-OVA IgG antibodies. The magnitude of the response of CQD and GO-PEG was comparable to that of using a commercial aluminum (Al) salt—based adjuvant in the form of aluminum oxyhydroxide (AlOOH). Immunization with ND resulted in significantly higher anti-OVA IgG antibody levels compared to the other nanostructures and AlOOH. Indeed, it reached a level comparable to CFA/IFA, known for its strong immune stimulation (despite known strong adjuvant propterties, CFA/IFA was forbidden for human use due to the lack of safely). In fact, using CFA/IFA resulted in the loss of one animal after immunization due to uncontrolled inflammation, providing the estimate of upper safe limits of triggered immune response. This was not the case using ND, as nanodiamonds were previously demonstrated by us to cause self-limiting inflammatory reaction [33]. None of the tested compounds was able to produce significant amount of anti-OVA IgM antibodies (as illustrated in Figure 3c). Motivated by these finding, ND were chosen and investigated in more details.

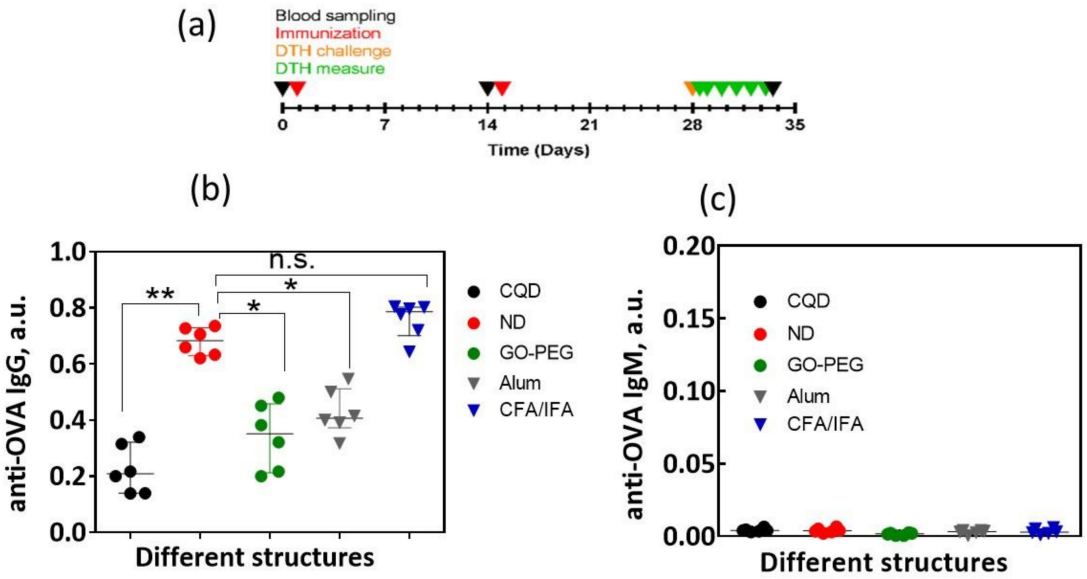

Figure 3. Immunization of mice with different nanostructures (1 mg) loaded with 50 μg OVA as model antigen: (**a**) experimental design. (**b**) humoral immune response determined by formed IgG against OVA antigen, serum dilution (1:5000). n.s. not significant, * $p = 0.01$ (significant), ** $p = 0.001$. (**c**) humoral immune response determined by formed anti-OVA IgM level in diluted (1:5000) serum.

2.2. Integration of HR2 Mimicking Peptide

Motivated by the findings of strong immunogenicity of ND, we hypothesized that its immune-bursting effect could be sufficient to stimulate immune response of the synthesized peptide. To achieve its molecular proximity to NDs and form the particulate antigen, the peptide was covalently attached to the NDs' surface via its cysteine residues at the N-terminus (as illustrated in Figure 4a). The success of the linkage was evidenced by XPS analysis (as illustrated in Figure 4b). Next to band at 285.0 eV due to diamond, band at 287.4 and 290.1 eV due respectively to maleimide and ester bonds are visible. Covalent immobilization of the peptide results in a strong decrease of the maleimide band at 287.4 eV (as illustrated in Figure 4c).

Since the peptide is modified in its N-terminus by a thiolated moiety, its antiviral capacity was determined against MERS-CoV pseudovirus (MERSpp) (as illustrated in Figure 4d). MERSpp mimics virus entry. Viral particles were incubated with the peptide at different doses prior the inoculation and during inoculation of Huh-7 cells for 2h. Inoculum and peptide were removed and cells were lysed 48h after infection. As shown in Figure 4d, the peptide was able to inhibit MERSpp infection in a dose-dependent manner, with and IC_{50} of 4.02 μg/mL, which is comparable to that obtained by Lu et al. [34].

2.3. Immune Response to ND-Pancoronaviral Peptide coNjugate in Mice

Humoral and cellular immune responses towards pancoronaviral peptide conjugated with ND were determined using Balc/c mice immunization model. Antipancoronaviral peptide antibodies of IgG and IgM types, were determined before immunization (day 0) as well as 14 and 32 days post immunization (as illustrated in Figure 5a). A strong humoral immune response was observed after a second immunization with the ND-pancoronaviral peptide. The measured titer of antibodies was 1/4000; the cutoff was set to 2.5× value of mock immunized control (as illustrated in Figure 5b). The nanostructures induced only minor increase in acute-phase antibodies of IgM type after 28 days, which we consider a beneficial factor, since excessive IgM formation can contribute to formation of immune complexes and subsequent kidney damage [35,36].

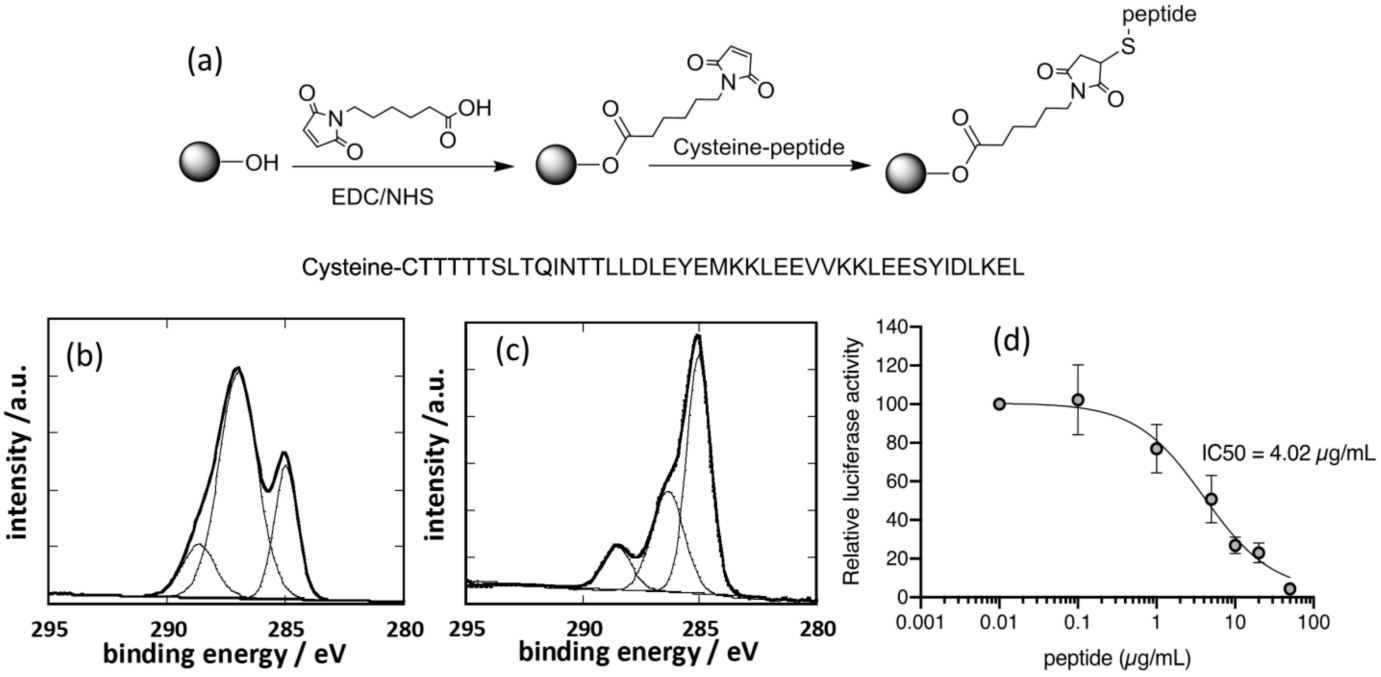

Figure 4. Preparation of peptide conjugated NDs: (**a**) Schematic illustration of synthesis of NDs carrying maleimide surface functions onto which the peptide was linked via its thiolated moiety at N-terminus. (**b**) C1s XPS spectrum of maleimide modified NDs. (**c**) C1s XPS spectrum of peptide modified NDs. (**d**) Antiviral activity of thiolated modified HR2 peptide. MERSpp were incubated with peptide at different concentrations for 30 min at RT prior to inoculation. Huh-7 cells were inoculated with MERSpp and peptide for 2 h, the inoculum was removed and replaced by culture medium for 46 h. Cells were lysed and luciferase activity quantified. Data are normalized relative to control without peptide and are expressed as mean ± SEM of 3 experiments.

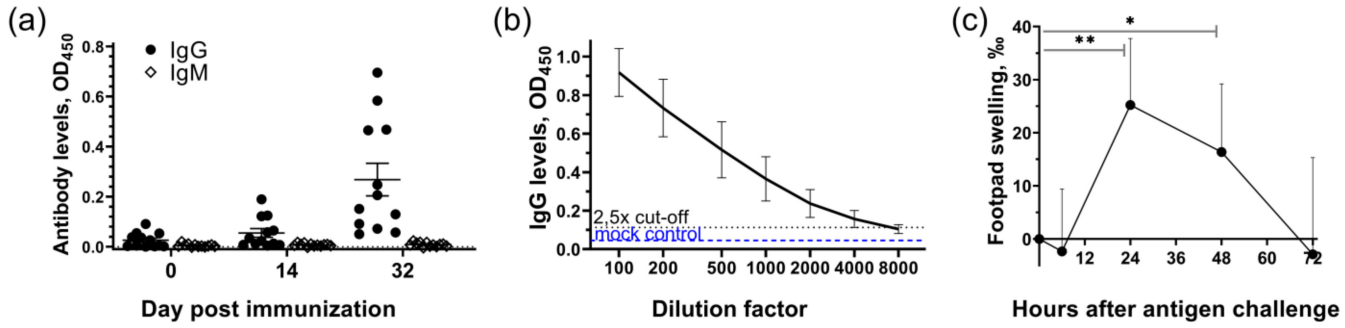

Figure 5. Immune (cellular and humoral) response in mice: (**a**) humoral immune response represented by levels of antipan-coronaviral IgG and IgM antibodies over course of immunization (done at day 0 and day 15), (**b**) titers of IgG antibodies directed against pancoronaviral peptide, (**c**) cellular immune response represented by delayed type hypersensitivity reaction measured by footpad swelling followed antigen injection into footpad. * $p < 0.05$, ** $p < 0.01$.

Delayed type hypersensitivity (DTH) reaction [37] was used for evaluation of cellular immune response using the proposed noninvasive model [21]. DTH is associated with Th1 reactivity (thus is a part of cellular immune response) to insoluble foreign antigens. The induced inflammatory reaction in the form of swelling is evaluated to judge on CD4+ T lymphocytes-mediated host immune response. The later promote T-helper cell type 1 (Th1) production of a soluble cytokine interferon-γ. After repeated contact with antigen, at day 28 mice were challenged with pancoronaviral peptide injected between the fingers of the footpad (right foot), non-specific reaction was caused by PBS injected to the left foot and served as control (as illustrated in Figure 5c). Footpad swelling dynamics was measured for 5 days, until swelling disappeared. Swell is usually proportional to the strength of

cellular activation. In the established setup DTH response was present and significant, reaching the peak response at 24 h. Based on the obtained data, we conclude that both humoral and cellular immune response were triggered by ND-pancoronaviral conjugate.

2.4. Activation of Neutrophil Extracellular Trap and Subsequent Sequestration

We recently demonstrated that in response to nanoparticles appearance in the body polymorphonuclear neutrophils (PMN) are activated to form neutrophil extracellular traps (NETs) [21], networks of externalized DNA produced with the aim to neutralize infection [38]. NETs release is followed by localized self-limiting inflammation, resulting in sequestration of inflammatory stimuli within NETs [39] and, as discovered recently, is an important trigger of alum action in vaccines [40]. NETs release and sequestration are responsible for the strong self-limiting and fast resolved inflammation caused by natural nanoparticles [39] like monosodium urate needle-like crystals at gout attack, to be as spontaneously resolved as it appears.

ND-pancoronaviral peptide conjugates provoked increased humoral immune response, thus we followed up the fate of the ND conjugate upon injection in the body. We tested the ability of NDs to stimulate NETs formation in human blood-derived PMNs. For this reason, venous blood from healthy volunteers served as a source for isolated PMNs. PMNs were placed in multiwell plate containing Sytox Green, a fluorescent dye, used to sense extracellular (or externalized) DNA, and NETs formation was evaluated in dynamics by externalization of DNA. Since outside of the body PMNs tend to activate to NETs foration spontaneously, a positive inducers of NETs formation - strong like phorbol mirystilacetate, PMA and weak, like 48 mM bicarbonate - were applied to cell well, simultaneously with the ND-pancoronaviral peptide conjugates. Figure 6a shows the typical data of neutrophil activation, isolated from a healthy donor. Mean fluorescence intensity (MFI) level of detected extracellular DNA suggests that ND-pancoronaviral peptide conjugates exhibit immediate to strong NET formation upon the contact with the isolated neutrophils, in good agreement with immunization data.

We further used air pouch model in laboratory mice [22], implying sterile air injected subcutaneously at the back of the animal to form a cavity, the later is being infiltrated with leukocytes followed by fluorescently-labeled NDs injection into the formed cavity (1 mg NDs per mouse). Within 24 h after NDs injection, animals were sacrificed, and their skin was assessed for NETs aggregates (as illustrated in Figure 6b). As can be seen from the figure, monocytes and neutrophils engulf ND particles, while the later also induce excessive DNA externalization with the formation of long DNA fibers. These NETs were shown to sequester nanoparticles in soft tissues [22].

To confirm NDs sequestration, CF790-labeled NDs were injected i.p. into swiss nude mice. The signal distribution was monitored during 5 days; after that, mice were sacrificed and organs were tested by fluorescence. Fluorescent signals were found in granuloma-like structure formed near the place of injection (as illustrated in Figure 6c,d). Subsequent histological staining demonstrated abundance of extracellular DNA. It could be concluded that, upon injection, neutrophils sequester nanoparticles, and due to sticky nature of DNA, they aggregate, protecting them from diffusion to surrounding tissues.

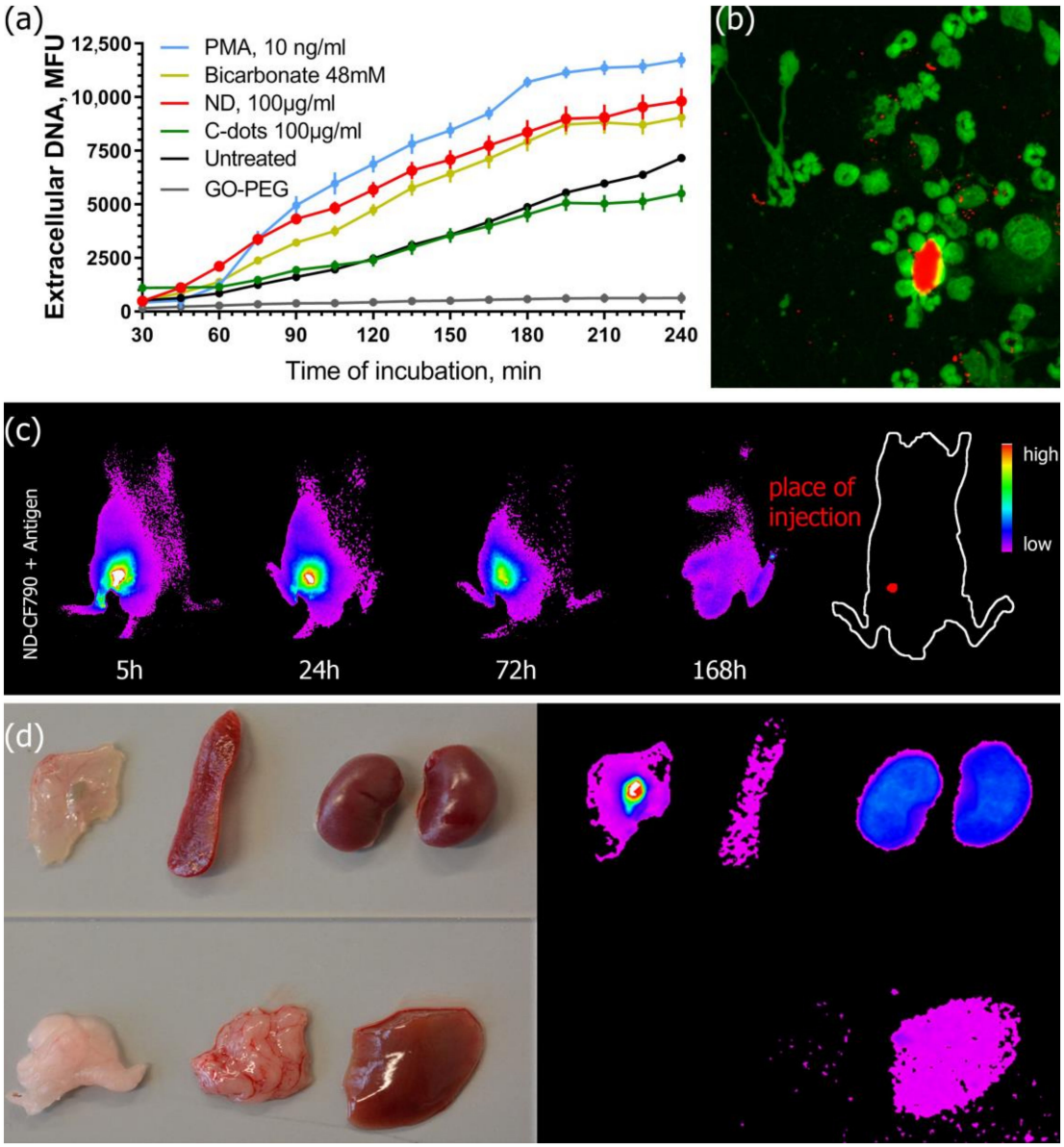

Figure 6. Immune response is mediated due to NETs; diamonds are sequestered in body parts. (**a**) externalization of DNA from isolated human polymorphonuclear neutrophils (PMN) cells upon contact with ND-pancoronaviral peptide conjugates (red), Phorbol mirystilacetate (PMA, positive control), bicarbonate (positive control), and untreated (negative control); (**b**) Fluorescence image of PMN cells (DNA stained green) engulfing ND-pancoronaviral peptide conjugates (red dots, injected into air-pouch of mice and cytosmears were made). Releasing DNA-containing fibers of NETs was observed in addition. (**c**) Time dependent fluorescence images: 1 mg of CF-790 labeled ND-peptide conjugates was injected intraperitoneally into swiss nude mice and fluorescence signal was monitored for 5 days. (**d**) Photographs and fluorescence images of internal organs after sacrificing the mice after 5 days: 1—granuloma-like tissue at place of injection, 2—spleen, 3—kidneys, 4—visceral fat, 5—intestine and 6—liver.

2.5. Duration of Immune Response in Rabbits

With the aim to evaluate the duration of immune response in animals, immunization of white rabbits with ND-pancoronaviral peptide, using CFA/IFA andjuvant as control, was performed (as illustrated in Figure 7a). Antibodies titres rised after 30 days in both cases, reaching the maximum shortly after. In the case of ND-pancoronaviral peptide, levels of IgG antibodies were steady for up to 120 days and more pronounced when compared to that of CFA/IFA adjuvant, measured at days 90 and 120. This is in line with typical laboratory rabbit immunization protocol, where absence of burst injections results

in antibody titre decline. The place of ND injection usually does not exhibit any strong swelling or abscesses (as illustrated in Figure 7b).

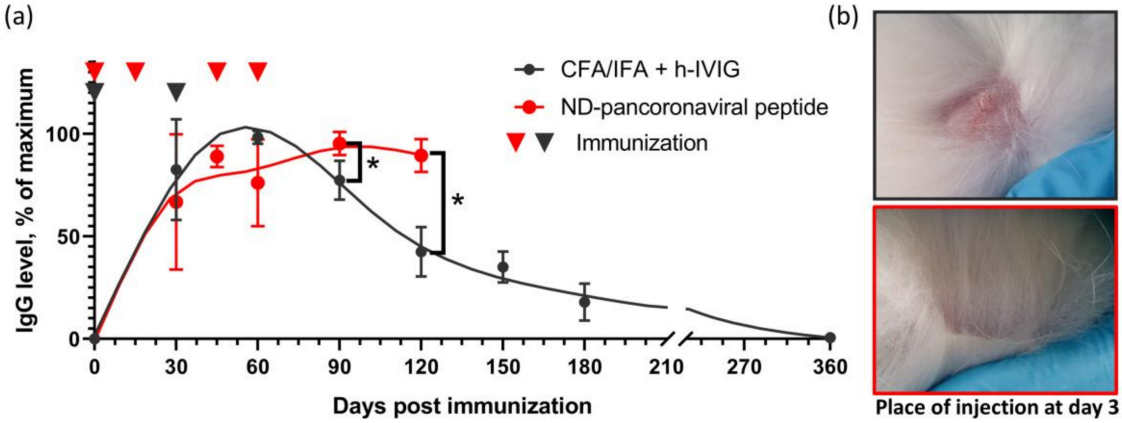

Figure 7. Antibodies induced by ND remained in rabbit blood for quite a long time. (**a**) Change of IgG level over time after post-immunization. Long-term observation of antibodies titers induced by 4 s.c. injections of ND-pancoronaviral peptide (red dots), as compared to standard 2 s.c. immunization using CFA/IFA adjuvant mixed with human intravenous immunoglobulin (IVIG) as mock antigen (grey). Data are normalized to maximum antibody levels. (**b**) CFA/IFA adjuvant is causing abscesses at place of injection, while no noticeable skin damage was observed after ND injection. * $p < 0.05$.

2.6. Cross-Reactivity of Peptide with Human Convalescent COVID Sera

To evaluate the usefulness of the approach, the possibility to induce immune response towards similar pathogen strains or mutated variants was investigated. We thus were intrigued to see if antibodies produced in patients after being infected with SARS-CoV-2 are able to recognize the pancoronaviral peptide. Convalescent COVID sera bind stronger to the pan-coronaviral peptide than sera of pre-COVID (before August 2019) controls, stored in our hospital's collection. The discriminative ability of pancoronaviral HR2 peptide versus receptor binding domain (RBD) of SARS-CoV-2 was evaluated in discrimination of the cohorts of convalescent COVID persons *vs.* those who never encountered both SARS-CoV-2 nor MERS viruses (as illustrated in Figure 8), $p < 0.001$ by Mann–Whitney test. Peptides were sorbed on plates and discrimination of convalescent COVID patients and pre-COVID controls was performed. The use of pancoronaviral peptide resulted in higher specificity but low sensitivity (as illustrated in Figure 8b), while RBD peptide resulted in higher sensitivity and lower specificity of detection (as illustrated in Figure 8c). In both cases AUROC was >80%, indicating that upon coronaviral infection there is plenty of antibodies formed targeting different parts of S-protein of the virus; thus, the use of peptides conserved among strains provides high benefits of inducing strong immune response towards currently unknown strains. Unfortunately, antibodies produced against the peptide were not able to neutralize MERSpp infection (data not shown), confirming that the HR2 region is not the major target of neutralizing antibodies. SARS-CoV-2 neutralizing antibodies target the receptor binding domain, and to a lesser extent, the region between HR1 and HR2 [41,42].

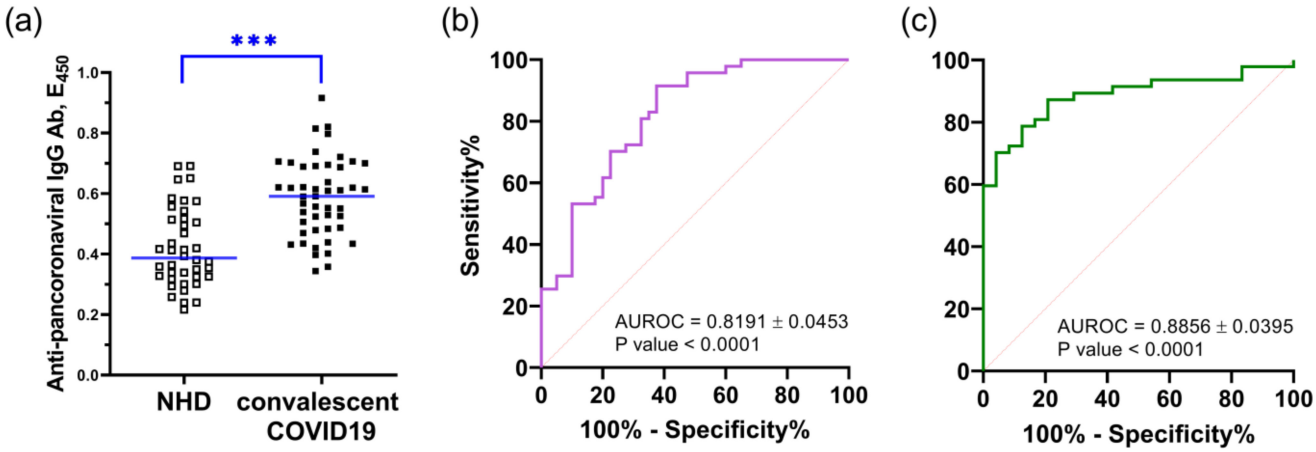

Figure 8. Cross-reactivity of peptide with human convalescent COVID sera: (**a**) Used pancoronaviral antigen is well-recognized by antibodies in convalescent COVID patients (**a**) and can be a potential immunization target. When pancoronaviral peptide was used as binding antigen for detection test, the following ROC curve (**b**) was obtained, as compared to ROC curve (**c**) when RBD peptide of S protein of SARS-CoV-2 was used as binding antigen for detection of antibody levels in human cohorts. NHD: normal healthy donors, blood collected before COVID pandemics, no MERS infection in medical history. *** $p < 0.001$.

3. Conclusions

Our data suggest that peptide-modified NDs seem to be well-adapted for boosting immunoresponse in mice and rabbits. The resulting immune response is rather strong and durable over time against new and emerging infections. Since the peptide of the pathogen can be relatively easily synthesized after sequencing the genetic information, the current approach can be valuable as an "emergency" vaccine to be made against newly emerging pathogens, exemplified with SARS-CoV-2 in the current work. Even if not providing the sterilizing immunity, the availability of long-lived antibody titers is undoubtedly beneficial. The components of vaccine such as nanoparticles and the machine for peptide synthesis can become the components of the remote missions to places with high risk of unknown infections and the ability of onsite vaccine manufacturing. The tendency of neutrophils, being present in both blood, tissues and patrolling body surfaces, to treat the nanoadjuvant as foreign object stimulates their activation for the production of neutrophil extracellular trap. The latter safely immobilize nanoadjuvant near the place of injection, with no trace found in circulation or major organs. The resulting granuloma-like formation serves as a safe depot of antigen and probably is a primary cause of prolonged immune response.

4. Materials and Methods

Reagents: citric acid, ethylenediamine, N-(3-dimethylaminopropyl)-N′-ethylcarbodiimide hydrochloride (EDC), N-hydroxysuccinimide (NHS), 6-maleimidohexanic acid, and sodium hydroxide were purchased from Sigma–Aldrich. The dialysis membranes were supplied by Spectrum Laboratories. Graphene oxide (GO) was obtained from Graphenea, Spain. Nanodiamonds were obtained from Aldrich (Diamond nanopowder, < 10 nm particle size, Nr. 636444, noted as $ND_{200\,nm}$ in this work) as well as from International Technology Center (Raleigh, NC, USA) noted as ND12 and from Adámas Nanotechnologies USA); notated as ND_5. Peptide XXTTTTTSLTQINTTLLDLEYEMKKLEEVVKKLEESYIDL KEL was obtained from ProtoGenics, France.

Synthesis of carbon quantum dots (CQD): CQD were synthesized following a method similar to that reported by Zhu et al. [43]. In brief, citric acid (2.1 g) and ethylenediamine (670 µL) were dissolved in Milli-Q water (20 mL). Then, the mixture was transferred into a Teflon-lined autoclave (125 mL acid digestion vessel no. 4748, Parr, France) and heated at 250 °C for 5 h. The resulting product was cooled to room temperature and dialyzed against

Milli-Q water using a cellulose ester dialysis membrane for 24 h (Biotech CE N°131093, pore size 500–1000 Da) to remove unreacted small molecules. The yield was about 40% and the stock solution was stored at 4 °C.

Synthesis of GO-PEG: Carboxylated GO (GO-COOH) was synthesized from GO as described by Sun et al. [31]. In short, sodium hydroxide (NaOH, 1.4 g) and chloroacetic acid (Cl-CH_2-COOH, 1 g) were added to 50 mL of an aqueous solution of GO (20 mg) and sonicated at 35 kHz for 2 h at 25 °C to convert hydroxyl groups present on GO to COOH via conjugation with acetic acid moieties. The GO-COOH solution was quenched with HCl (20 %), washed (four times) with distilled water until neutral pH, and purified by repeated cycles of centrifugation (3000 *g*, 20 min)/rinsing. PEGylation was performed by mixing 1 mL of GO-COOH in water (1 mg/mL) with NH_2PEGNH_2 (3 mg, 1.5 kDa) in the presence of EDC (0.2 g) and maintaining the reaction mixture for 2 h in a sonication bath (35 kHz) at 30 °C. Thereafter, the reaction mixture was quenched by mercaptoethanol and the product was dialyzed using a 12–14 MWCO membrane (3 × 500 mL Milli-Q water). The resulting suspension was centrifuged at 400,000 *g*. for 1 h to remove large aggregates. The solution was filtered using a 35 kDa cutoff membrane and then resuspended in the desired volume of PBS to prepare GO-PEG of around ~2 mg/mL.

Surface modification: ND (10 mg) particles were mixed with a solution of NHS/EDC (40 mM) and 6-meleimidohexanoic acid (33 mM) in PBS 1× and kept reacting for 3 days at room temperature. The formed maleimide-modified particles were washed by centrifugation (13,000 *g* for 2 min.). To ND-maleimide particles (1 mg mL^{-1}) in PBS 1× was added 1 mg of peptide and the mixture was kept for 2h at room temperature. The formed ND-peptide particles were washed by centrifugation (13,000 *g* for 2 min) and resuspended in PBS 1× (1 mg/mL) and kept at 4 °C before use.

Characterization: X-ray Photoelectron Spectroscopy (XPS) measurements were carried out using ESCALAB 220 XL spectrometer from Vacuum Generators featuring a monochromatic Al Kα X-ray source (1,486.6 eV) and a spherical energy analyzer operated in the CAE (constant analyzer energy) mode (CAE = 100 eV for survey spectra and CAE = 40 eV for high-resolution spectra), using the electromagnetic lens mode. The angle between the incident X-rays and the analyzer is 58° and the detection angle of the photoelectrons is 30°. Transmission Electron Microscopy (TEM) images were recorded on a JEOL JEM-2800 electron microscope operated at an accelerating voltage of 200 kV. The average hydrodynamic diameter, the polydispersity index (PDI), and the zeta-potential were recorded on a Zetasizer® Nano ZS (Malvern Instruments S.A., Worcestershire, UK). All the batches were diluted to 100 μg mL^{-1} in water and analyzed in triplicate at 37 °C.

Cell and Toxicity Assay: The cell lines HeLa and Huh-7 used in the study were from ATCC collection. Cells were cultured and maintained in Dulbecco's Modified Eagle's medium (DMEM, Gibco®) supplemented with 10% fetal bovine serum (FBS, Gibco®) and 1% penicillin-streptomycin (Gibco®) in a humidified incubator at 37 °C and 5% CO_2. Cells were seeded at a density of 15 × 10^3 cells/well in a 96-well plate and grown for 24 h before assay. The culture medium was replaced with a fresh medium that contains increasing concentrations (1 to 100 μg mL−1) of nanomaterial of interest for 2 h and 8 h. Then, the old medium was aspirated, and cells were washed with PBS. The cell viability was evaluated using resazurin cell viability assay. Briefly, 100 μL of the resazurin solution (11 μg mL^{-1}) in DMEM/10% FBS were added to each well and the plate was incubated for 4 h in the humidified incubator. The fluorescence emission of each well was measured at 593 nm (20-nm bandwidth) with an excitation at 554 nm (18-nm bandwidth) using a Cytation™ 5 Cell Imaging Multi-Mode Reader (BioTek Instruments SAS, Colmar, France). Each condition was replicated three times and the mean fluorescence value of nonexposed cells was taken as 100% cellular viability.

MERSpp antiviral assay. Particles pseudotyped with MERS-CoV-S envelope proteins (MERSpp) were produced, as previously described [44]. Pseudotyped virions were incubated with the peptide for 30 min and were used to inoculate Huh-7 cells in 96-well plates for 2 h. The inoculum was removed and cells were further incubated with culture medium

for 46 h. Cells were lysed and luciferase activity was detected by using a Luciferase Assay kit (Promega) and light emission measured by using a Tristar LB 941 luminometer (Berthold Technologies).

Animals. Studies involving animals, including housing and care, method of euthanasia, and experimental protocols were approved by the Ethical committee of Danylo Halytsky Lviv National Medical University, protocols 20191216/10, 20180226/2, 20170223/5 & 20130624/6, all experiments were designed to comply with principles of the 3Rs (Replacement, Reduction and Refinement). Studies involving laboratory rabbits were performed under the supervision of a certified veterinary doctor. Twelve white laboratory rabbits, 4-month old males were used for this investigation. Rabbits were housed in individual cages in a temperature/humidity/light-controlled environment, with both food and drinking water available ad libitum. Ex vivo fluorescent imaging of mice was performed as described in [45].

Animal immunization. Mice immunization was done as described previously [23], rabbit immunization was performed as described in [46]. Either a mixture of nanoparticles with model antigen ovalbumin (OVA) in case of mice or human IVIG (for rabbits), or conjugates of ND with pancoronaviral peptide were used for immunization. The DTH test was performed 28 days after the 1st immunization by injection of 50 μL of OVA / peptide in PBS (100 μg mL^{-1}) into the right hind paw. Injection of 50 μL of PBS into the left hind paw was used as a control. The thickness of the paw was measured with a caliper (B110T; Kroeplin Laengenmesstechnik) before the injection and 6, 24, 48, 72 and 96 h after injection, as described previously [23]. Blood was collected from mouse tail before experiment start (day 0), before second immunization (day 14) and at the end of experiment (day 35). No more than 50 μL of blood was collected to prevent damage to the animal. Serum was isolated (usually 20 μL per mice) and immediately frozen. Blood was collected from rabbit ear vein, no more than 2 mL, at the indicated time of experiment, with the interval between bleeding no less than 14 days.

The air pouch model was performed by injection of 5 mL of sterile air subcutaneously into the back of Balb/c mice [47]. After two days, an additional 2 mL of sterile air were injected into the pouch. Two days later, 5 mg of n/μP in PBS or PBS only were injected. 24 h later, mice were sacrificed, and the air pouch membranes were analyzed. Cells of air pouch were analyzed using fluorescent microscopy as described in [48].

Patient cohorts. Analyses of human materials were approved by the Ethics Committees of Danylo Halytsky Lviv National Medical University (DH LNMU No.5/2017-02-23). The current study involved 55 samples from SARS-CoV-2 infected patients treated in the Lviv Regional Clinical Infection Hospital of Infectious Diseases / Department of Infectious Diseases, Danylo Halytsky Lviv National Medical University (Lviv, Ukraine) during April–August 2020. Written informed consent was obtained from every person before blood collection. All patients were PCR-positive upon hospitalization. Sera collection took place at least 3 weeks after the appearance of clinical symptoms when a person was recovered. Recovery was assessed by (a) disappearance of clinical symptoms, (b) negative PCR tests. All sera collected were tested positive for anti-SARS-CoV-2 antibodies using reference detection test from Xema (Xema Medica, Ukraine); in this test, a mixture of spike and nucleocapside antigens served as antigen. Cohort of patients consisted of 29 males and 26 females, the disease course was mild in 11 cases (20.0%), moderate in 28 (50.9%) and severe in 16 cases (29.1%); the later were associated with age >60 y.o. and accompanying chronic illnesses. For most cases, incubation period lasted 5–14 days. None of the patients had a history of MERS-CoV infection.

A group of normal healthy donors (NHD) who donated blood between June and November 2019 (pre-COVID-19) served as controls; they were both age- and sex-matched to fit the study group. None of the healthy donors had a history of MERS-CoV infection. Informed written consent for blood withdrawal was obtained from each patient and NHD.

ELISA tests. Sera samples from convalescent COVID-19 patients and NHDs were frozen at −20 °C. For testing anti-MERS response, immunosorbent NUNC maxisorp plates

(Thermo Scientific, Waltham, MA, USA) were coated with pancoronaviral peptide (50 µL of a 4 µg/mL solution) in a carbonate-bicarbonate buffer (100 mM, pH 9.6). For testing anti-SARS-CoV-2 response, immunosorbent NUNC MaxiSorp plates (Thermo Scientific, Waltham, MA, USA) were coated with recombinant RBD domain of spike protein of SARS-CoV-2, (Xema Medica, Ukraine). All serum samples were diluted 1:1000 in the carbonate-bicarbonate buffer and incubated at 37 °C for 1 h, after that the plates were washed again. For determination of IgG antibody, titre samples collected at day 35, after second immunization, were diluted 1:100, 1:200, 1:500, 1:1000, 1:2000, 1:4000, 1:8000, 1:16,000, 1:32,000, 1:64,000, and 1:128,000. Goat antihuman IgG (H+L)-horseradish peroxidase (HRP) (109-035-003, Jackson ImmunoResearch) was diluted in washing buffer (1:25,000), added to the plates, and incubated at room temperature for 1 h. After the corresponding washings, the assay was developed with 3,3′,5,5′-tetramethylbenzidine (TMB) containing an excess of H_2O_2 as a substrate (50 µL per well). The reaction was stopped with 50 µL/well of sulfuric acid (1 M). The absorbance was read at 450 nm/600 nm using a Perkin Elmer BioAssay reader HST700 (Waltham, MA, USA). Anti-SARS-CoV-2 ELISA was additionally tested with reference positive sera for COVID-19 diagnostics, and their signal was in the range of 0.45–0.60 OD. The coefficient of variation between replicates was controlled to be <3%. Other ELISA parameters were controlled, according to the best practice of ELISA analysis [49,50] and our previous reports [51,52].

Analysis of DNA Externalization. Human granulocytes were isolated from heparinized venous blood of normal healthy donors by Lymphoflot (Bio-Rad) density gradient centrifugation, as described [36]. The granulocyte-rich layer on top of RBCs was taken and subjected to hypotonic lysis of RBCs. Isolated granulocytes were cultured in 96-well culture plates at 5×10^6 cells per milliliter with special inducers of NETosis and with the fluorescent nucleic acid dye Sytox green (Life Technologies). The kinetics were measured for 3 h using BioAssay Reader HTS7000 Plus (Perkin Elmer), excitation 480/15 nm, emission 535/20 nm.

Bioinformatics. The protein homology searches were done using blast (NCBI) and PDB databases. To include the regions with resolved structures in our searches, we had used SEQATOMS (http://www.bioinformatics.nl/tools/seqatoms/ using later update of 12 March 2021) [53]. Protein structures were visualized and aligned using PyMOL (https://pymol.org/, accessed on 12 March 2021).

Data analysis. ELISA testing was performed in duplicate using 2 technical replicates for each analysis (coefficient of variation [CV] always <3%). The data were normalized between plates using positive controls and corrected for background signal of secondary antibodies on each plate, then the mean values were calculated. The mean values were used to construct data on the figures. For comparisons between two groups, the Mann–Whitney U-test for numerical variables was used. A receiver operating characteristic (ROC) curve was generated. The area under the ROC (AUROC) was calculated to estimate the specificity, sensitivity, and usefulness of the binding assays. All analyses were performed using Excel 2016 (Microsoft Corp., Redmond, WA, USA) and Prism 8.2 (GraphPad, San Diego, CA, USA) software. A p-value of ≤ 0.05 was considered statistically significant. Four levels of significance are depicted in the figures by asterisks: * $p < 0.05$; ** $p < 0.01$; *** $p < 0.001$; *** $p < 0.0001$.

Supplementary Materials: The following are available online at https://www.mdpi.com/article/10.3390/pathogens10070861/s1, Figure S1: sequence alignment of the HR2 region of coronaviruses. Figure S2: low-dimension carbon-based nanostructures investigated in this work. Figure S3: cell viability of the different nanostructures.

Author Contributions: Conceptualization, R.B. (Rostyslav Bilyy) and S.S.; methodology, Q.P., N.F., G.B., R.G., Y.L.; validation, Q.P., A.B., N.F. and Y.L.; resources, R.B. (Rostyslav Bilyy) and S.S.; writing—original draft preparation, R.B. (Rabah Boukherroub), K.S. and S.S.; writing—review and editing, R.B. (Rostyslav Bilyy), R.B. (Rabah Boukherroub), S.B., J.D.; supervision, R.B. (Rostyslav Bilyy) and S.S. project administration, R.B. (Rostyslav Bilyy) and S.S.; funding acquisition, S.S. and R.B. (Rostyslav Bilyy). All authors read and agreed to the published version of the manuscript.

Funding: This research was funded by the Centre National de la Recherche Scientifique (CNRS), the University of Lille, the ANR, the CPER "Photonics for Society" and the Agence Nationale de la Recherche (ANR-nanoMERS). Financial support from the Grant of Ministry of Healthcare of Ukraine 0119U101338 and National Research Foundation of Ukraine 2020.02/0131; Volkswagen-Stiftung grant No 97744. This project has received funding from the European Union's Horizon 2020 research and innovation program under grant agreements No 861878.

Institutional Review Board Statement: All animal experiments were designed to comply with principles of the 3Rs (Replacement, Reduction and Refinement) and approved by Ethical committee of Danylo Halytsky Lviv National Medical University, protocols 20191216/10, 20180226/2, 20170223/5 & 20130624/6; Study of remnants of human materials were approved by the Ethics Committees of Danylo Halytsky Lviv National Medical University (DH LNMU No.5/2017-02-23).

Informed Consent Statement: Informed consent was obtained from all subjects involved in the study before sample collection.

Data Availability Statement: PDB SEQATOMS database used in the study is available at https://www.bioinformatics.nl/tools/seqatoms/blast.html, accessed on 12 March 2021.

Acknowledgments: Andrii Rabets for technical assistance, V'yacheslav Lehen'kyi for help with animal imaging, Ihor Bernyk for help with sample collection.

Conflicts of Interest: The authors declare no conflict of interest.

References

1. Plotkina, S.A. Vaccination against the major infectious diseases. *Comptes Rendus l'Académie des Sci.-Ser. III-Sci. la Vie* **1999**, *322*, 943–951. [CrossRef]
2. Shen, A.K.; Cooke, M.T. Infectious disease vaccines. *Nat. Rev. Drug Discov.* **2019**, *18*, 169–170. [CrossRef]
3. Arvin, A.M.; Fink, K.; Schmid, M.A.; Cathcart, A.; Spreafico, R.; Havenar-Daughton, C.; Lanzavecchia, A.; Corti, D.; Virgin, H.W. A perspective on potential antibody-dependent enhancement of SARS-CoV-2. *Nature* **2020**, *584*, 353–363. [CrossRef]
4. Welsh, R.M.; Fujinami, R.S. Pathogenic epitopes, heterologous immunity and vaccine design. *Nat. Rev. Microbiol.* **2007**, *5*, 555–563. [CrossRef] [PubMed]
5. van Riel, D.; de Wit, E. Next-generation vaccine platforms for COVID-19. *Nat. Mater.* **2020**, *19*, 810–812. [CrossRef] [PubMed]
6. Malonis, R.J.; Lai, J.R.; Vergnolle, O. Peptide-Based Vaccines: Current Progress and Future Challenges. *Chem. Rev.* **2020**, *120*, 3210–3229. [CrossRef]
7. Maiti, D.; Tong, X.; Mou, X.; Yang, K. Carbon-Based Nanomaterials for Biomedical Applications: A Recent Study. *Front. Pharmacol.* **2019**, *9*, 1401. [CrossRef] [PubMed]
8. Patel, K.D.; Singh, R.K.; Kim, H.-W. Carbon-based nanomaterials as an emerging platform for theranostics. *Mater. Horizons* **2019**, *6*, 434–469. [CrossRef]
9. Cha, C.; Shin, S.R.; Annabi, N.; Dokmeci, M.R.; Khademhosseini, A. Carbon-Based Nanomaterials: Multifunctional Materials for Biomedical Engineering. *ACS Nano* **2013**, *7*, 2891–2897. [CrossRef]
10. Nekoueian, K.; Amiri, M.; Sillanpää, M.; Marken, F.; Boukherroub, R.; Szunerits, S. Carbon-based quantum particles: An electroanalytical and biomedical perspective. *Chem. Soc. Rev.* **2019**, *48*, 4281–4316. [CrossRef]
11. Zhang, X.; Hu, W.; Li, J.; Tao, L.; Wei, Y. A comparative study of cellular uptake and cytotoxicity of multi-walled carbon nanotubes, graphene oxide, and nanodiamond. *Toxicol. Res.* **2012**, *1*, 62–68. [CrossRef]
12. Mochalin, V.N.; Shenderova, O.; Ho, D.; Gogotsi, Y. The properties and applications of nanodiamonds. *Nat. Nanotechnol.* **2012**, *7*, 11–23. [CrossRef] [PubMed]
13. Barras, A.; Martin, F.A.; Bande, O.; Baumann, J.-S.; Ghigo, J.-M.; Boukherroub, R.; Beloin, C.; Siriwardena, A.; Szunerits, S. Glycan-functionalized diamond nanoparticles as potent E. coli anti-adhesives. *Nanoscale* **2013**, *5*, 2307. [CrossRef]
14. Turcheniuk, V.; Turcheniuk, K.; Bouckaert, J.; Barras, A.; Dumych, T.; Bilyy, R.; Zaitsev, V.; Siriwardena, A.; Wang, Q.; Boukherroub, R.; et al. Affinity of Glycan-Modified Nanodiamonds towards Lectins and Uropathogenic Escherichia Coli. *ChemNanoMat* **2016**, *2*, 307–314. [CrossRef]
15. Khanal, M.; Larsonneur, F.; Raks, V.; Barras, A.; Baumann, J.S.; Martin, F.A.; Boukherroub, R.; Ghigo, J.M.; Ortiz Mellet, C.; Zaitsev, V.; et al. Inhibition of type 1 fimbriae-mediated Escherichia coli adhesion and biofilm formation by trimeric cluster thiomannosides conjugated to diamond nanoparticles. *Nanoscale* **2015**, *7*, 2325–2335. [CrossRef]
16. Khanal, M.; Vausselin, T.; Barras, A.; Bande, O.; Turcheniuk, K.; Benazza, M.; Zaitsev, V.; Teodorescu, C.M.; Boukherroub, R.; Siriwardena, A.; et al. Phenylboronic-Acid-Modified Nanoparticles: Potential Antiviral Therapeutics. *ACS Appl. Mater. Interfaces* **2013**, *5*, 12488–12498. [CrossRef] [PubMed]
17. Irvine, D.J.; Hanson, M.C.; Rakhra, K.; Tokatlian, T. Synthetic Nanoparticles for Vaccines and Immunotherapy. *Chem. Rev.* **2015**, *115*, 11109–11146. [CrossRef]

18. Zhao, L.; Seth, A.; Wibowo, N.; Zhao, C.-X.; Mitter, N.; Yu, C.; Middelberg, A.P.J. Nanoparticle vaccines. *Vaccine* **2014**, *32*, 327–337. [CrossRef]
19. Kossovsky, N.; Gelman, A.; Hnatyszyn, H.J.; Rajguru, S.; Garrell, R.L.; Torbati, S.; Freitas, S.S.F.; Chow, G.-M. Surface-Modified Diamond Nanoparticles as Antigen Delivery Vehicles. *Bioconjug. Chem.* **1995**, *6*, 507–511. [CrossRef]
20. Pham, N.B.; Ho, T.T.; Nguyen, G.T.; Le, T.T.; Le, N.T.; Chang, H.C.; Pham, M.D.; Conrad, U.; Chu, H.H. Nanodiamond enhances immune responses in mice against recombinant HA/H7N9 protein. *J. Nanobiotechnology* **2017**, *15*, 1–12. [CrossRef]
21. Muñoz, L.E.; Bilyy, R.; Biermann, M.H.C.; Kienhöfer, D.; Maueröder, C.; Hahn, J.; Brauner, J.M.; Weidner, D.; Chen, J.; Scharin-Mehlmann, M.; et al. Nanoparticles size-dependently initiate self-limiting NETosis-driven inflammation. *Proc. Natl. Acad. Sci.* **2016**, *113*, E5856–E5865. [CrossRef]
22. Bilyy, R.; Bila, G.; Vishchur, O.; Vovk, V.; Herrmann, M. Neutrophils as Main Players of Immune Response Towards Nondegradable Nanoparticles. *Nanomaterials* **2020**, *10*, 1273. [CrossRef]
23. Bilyy, R.; Paryzhak, S.; Turcheniuk, K.; Dumych, T.; Barras, A.; Boukherroub, R.; Wang, F.; Yushin, G.; Szunerits, S. Aluminum oxide nanowires as safe and effective adjuvants for next-generation vaccines. *Mater. Today* **2019**, *22*, 58–66. [CrossRef]
24. Lu, L.; Liu, Q.; Zhu, Y.; Chan, K.-H.H.; Qin, L.; Li, Y.; Wang, Q.; Chan, J.F.-W.W.; Du, L.; Yu, F.; et al. Structure-based discovery of Middle East respiratory syndrome coronavirus fusion inhibitor. *Nat. Commun.* **2014**, *5*, 3067. [CrossRef]
25. Rabets, A.; Bila, G.; Grytsko, R.; Samborsky, M.; Rebets, Y.; Vari, S.; Pagneux, Q.; Barras, A.; Boukherroub, R.; Szunerits, S.; et al. Development of antibodies to pan-coronavirus spike peptides in convalescent COVID-19 patients. *medRxiv* **2020**. [CrossRef]
26. Rabets, A.; Bila, G.; Grytsko, R.; Samborskyy, M.; Rebets, Y.; Vari, S.G.; Pagneux, Q.; Barras, A.; Boukherroub, R.; Szunerits, S.; et al. The Potential of Developing Pan-Coronaviral Antibodies to Spike Peptides in Convalescent COVID-19 Patients. *Arch. Immunol. Ther. Exp.* **2021**, *69*, 5. [CrossRef] [PubMed]
27. Yuan, Y.; Cao, D.; Zhang, Y.; Ma, J.; Qi, J.; Wang, Q.; Lu, G.; Wu, Y.; Yan, J.; Shi, Y.; et al. Cryo-EM structures of MERS-CoV and SARS-CoV spike glycoproteins reveal the dynamic receptor binding domains. *Nat. Commun.* **2017**, *8*, 15092. [CrossRef] [PubMed]
28. Łoczechin, A.; Séron, K.; Barras, A.; Giovanelli, E.; Belouzard, S.; Chen, Y.-T.; Metzler-Nolte, N.; Boukherroub, R.; Dubuisson, J.; Szunerits, S. Functional Carbon Quantum Dots as Medical Countermeasures to Human Coronavirus. *ACS Appl. Mater. Interfaces* **2019**, *11*, 42964–42974. [CrossRef]
29. Huang, X.; Li, M.; Xu, Y.; Zhang, J.; Meng, X.; An, X.; Sun, L.; Guo, L.; Shan, X.; Ge, J.; et al. Novel Gold Nanorod-Based HR1 Peptide Inhibitor for Middle East Respiratory Syndrome Coronavirus. *ACS Appl. Mater. Interfaces* **2019**, *11*, 19799–19807. [CrossRef] [PubMed]
30. Williams, O.A.; Hees, J.; Dieker, C.; Jäger, W.; Kirste, L.; Nebel, C.E. Size-Dependent Reactivity of Diamond Nanoparticles. *ACS Nano* **2010**, *4*, 4824–4830. [CrossRef]
31. Sun, X.; Liu, Z.; Welsher, K.; Robinson, J.T.; Goodwin, A.; Zaric, S.; Dai, H. Nano-graphene oxide for cellular imaging and drug delivery. *Nano Res.* **2008**, *1*, 203–212. [CrossRef] [PubMed]
32. Kong, N.; Jiang, T.; Zhou, Z.; Fu, J. Cytotoxicity of polymerized resin cements on human dental pulp cells in vitro. *Dent. Mater.* **2009**, *25*, 1371–1375. [CrossRef] [PubMed]
33. Biermann, M.H.C.; Podolska, M.J.; Knopf, J.; Reinwald, C.; Weidner, D.; Maueröder, C.; Hahn, J.; Kienhöfer, D.; Barras, A.; Boukherroub, R.; et al. Oxidative burst-dependent NETosis is implicated in the resolution of necrosis-associated sterile inflammation. *Front. Immunol.* **2016**, *7*. [CrossRef] [PubMed]
34. Lu, S.; Wang, Y.; Chen, Y.; Wu, B.; Qin, K.; Zhao, J.; Lou, Y.; Tan, W. Discovery of a novel canine respiratory coronavirus support genetic recombination among betacoronavirus1. *Virus Res.* **2017**, *237*, 7–13. [CrossRef] [PubMed]
35. Stümer, J.; Biermann, M.H.C.H.C.; Knopf, J.; Magorivska, I.; Kastbom, A.; Svärd, A.; Janko, C.; Bilyy, R.; Schett, G.; Sjöwall, C.; et al. Altered glycan accessibility on native immunoglobulin G complexes in early rheumatoid arthritis and its changes during therapy. *Clin. Exp. Immunol.* **2017**, *189*, 372–382. [CrossRef] [PubMed]
36. Platt, J.L.; Cascalho, M. IgM in the kidney: A multiple personality disorder. *Kidney Int.* **2015**, *88*, 439–441. [CrossRef]
37. Allen, I.C. Delayed-type hypersensitivity models in mice. *Methods Mol Biol* **2013**, *1031*, 101–107. [CrossRef] [PubMed]
38. Brinkmann, V.; Reichard, U.; Goosmann, C.; Fauler, B.; Uhlemann, Y.; Weiss, D.S.; Weinrauch, Y.; Zychlinsky, A. Neutrophil extracellular traps kill bacteria. *Science (80-.)* **2004**, *303*, 1532–1535. [CrossRef] [PubMed]
39. Schauer, C.; Janko, C.; Munoz, L.E.L.E.; Zhao, Y.Y.; Kienhöfer, D.; Frey, B.; Lell, M.; Manger, B.; Rech, J.; Naschberger, E.; et al. Aggregated neutrophil extracellular traps limit inflammation by degrading cytokines and chemokines. *Nat. Med.* **2014**, *20*, 511–517. [CrossRef] [PubMed]
40. Stephen, J.; Scales, H.E.; Benson, R.A.; Erben, D.; Garside, P.; Brewer, J.M. Neutrophil swarming and extracellular trap formation play a significant role in Alum adjuvant activity. *NPJ Vaccines* **2017**, *2*, 1. [CrossRef]
41. Zost, S.J.; Gilchuk, P.; Case, J.B.; Binshtein, E.; Chen, R.E.; Nkolola, J.P.; Schäfer, A.; Reidy, J.X.; Trivette, A.; Nargi, R.S.; et al. Potently neutralizing and protective human antibodies against SARS-CoV-2. *Nature* **2020**, *584*, 443–449. [CrossRef] [PubMed]
42. Li, Y.; Lai, D.; Zhang, H.; Jiang, H.; Tian, X.; Ma, M.; Qi, H.; Meng, Q.; Guo, S.; Wu, Y.; et al. Linear epitopes of SARS-CoV-2 spike protein elicit neutralizing antibodies in COVID-19 patients. *Cell. Mol. Immunol.* **2020**, *17*, 1095–1097. [CrossRef]
43. Zhu, S.; Meng, Q.; Wang, L.; Zhang, J.; Song, Y.; Jin, H.; Zhang, K.; Sun, H.; Wang, H.; Yang, B. Highly Photoluminescent Carbon Dots for Multicolor Patterning, Sensors, and Bioimaging. *Angew. Chem. Int. Ed.* **2013**, *52*, 3953–3957. [CrossRef]
44. Belouzard, S.; Chu, V.C.; Whittaker, G.R. Activation of the SARS coronavirus spike protein via sequential proteolytic cleavage at two distinct sites. *Proc. Natl. Acad. Sci. USA* **2009**, *106*, 5871–5876. [CrossRef]

45. Turcheniuk, K.; Dumych, T.; Bilyy, R.; Turcheniuk, V.; Bouckaert, J.; Vovk, V.; Chopyak, V.; Zaitsev, V.; Mariot, P.; Prevarskaya, N.; et al. Plasmonic photothermal cancer therapy with gold nanorods/reduced graphene oxide core/shell nanocomposites. *RSC Adv.* **2016**, *6*, 1600–1610. [CrossRef]
46. ThermoFisherScientific Custom Rabbit Polyclonal Antibody Production Protocols. Available online: https://www.thermofisher.com/ua/en/home/life-science/antibodies/custom-antibodies/custom-antibody-production/custom-polyclonal-antibody-production/custom-rabbit-polyclonal-antibody-production-protocols.html (accessed on 2 July 2019).
47. Sin, Y.M.; Sedgwick, A.D.; Chea, E.P.; Willoughby, D.A. Mast cells in newly formed lining tissue during acute inflammation: A six day air pouch model in the mouse. *Ann. Rheum. Dis.* **1986**, *45*, 873–877. [CrossRef]
48. Bila, G.; Schneider, M.; Peshkova, S.; Krajnik, B.; Besh, L.; Lutsyk, A.; Matsyura, O.; Bilyy, R. Novel approach for discrimination of eosinophilic granulocytes and evaluation of their surface receptors in a multicolor fluorescent histological assessment. *Ukr. Biochem. J.* **2020**, *92*, 99–106. [CrossRef]
49. Kiessig, S.; Abel, U.; Risse, P.; Friedrich, J.; Heinz, F.; Kunz, C. Problems of cut-off level determination in enzyme immunoassays: The case of TBE-ELISA. *Klin. Lab.* **1993**, *39*, 877–886.
50. Crowther, J.R. *The ELISA Guidebook*; Methods in Molecular Biology; Humana Press: Totowa, NJ, USA, 2009; Volume 516, ISBN 978-1-60327-253-7.
51. Biermann, M.H.C.C.; Boeltz, S.; Pieterse, E.; Knopf, J.; Rech, J.; Bilyy, R.; van der Vlag, J.; Tincani, A.; Distler, J.H.W.W.; Krönke, G.; et al. Autoantibodies Recognizing Secondary NEcrotic Cells Promote Neutrophilic Phagocytosis and Identify Patients With Systemic Lupus Erythematosus. *Front. Immunol.* **2018**, *9*, 989. [CrossRef] [PubMed]
52. Bozhenko, M.; Boichuk, M.; Bila, G.; Nehrych, T.; Bilyy, R. Freezing influences, the exposure of IgG glycans in sera from multiple sclerosis patients. *Ukr. Biochem. J.* **2020**, *92*, 21–31. [CrossRef]
53. Brandt, B.W.; Heringa, J.; Leunissen, J.A.M. SEQATOMS: A web tool for identifying missing regions in PDB in sequence context. *Nucleic Acids Res.* **2008**, *36*, W255–W259. [CrossRef] [PubMed]